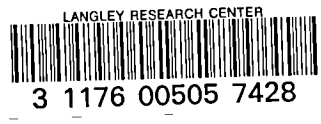

NASA-TM-84259 19820020701

Numerical Simulation of Wall-Bounded Turbulent Shear Flows

Parviz Moin

June 1982

NASA
National Aeronautics and
Space Administration

NASA Technical Memorandum 84259

Numerical Simulation of Wall-Bounded Turbulent Shear Flows

Parviz Moin, Ames Research Center, Moffett Field, California

National Aeronautics and
Space Administration

Ames Research Center
Moffett Field, California 94035

NUMERICAL SIMULATION OF WALL-BOUNDED TURBULENT SHEAR FLOWS

Parviz Moin

NASA Ames Research Center
Moffett Field, California 94035 U.S.A.

1. Introduction

Advances in computer hardware and numerical methods in conjunction with carefully designed computer programs have made meaningful numerical simulation of wall-bounded turbulent flows possible. The physical realism of the resultant computer-generated data has been validated by detailed structural and statistical comparisons with experimental measurements. These calculations have proven to be a very useful complement to the laboratory experiments.

This paper reviews some recent developments in three-dimensional, time-dependent numerical simulation of turbulent flows bounded by a wall. We shall be considering both direct and large-eddy simulation techniques within the same computational framework. In the following section, we have outlined the governing equations. In Section 3, the computational spatial-grid requirements as dictated by the known structure of turbulent boundary layers are presented. Next, we review the numerical methods currently in use. Some of the features of these algorithms, including spatial differencing, time advancement, and data management, will be discussed in some detail. In Section 5 we provide a selection of the results of recent calculations of turbulent channel flow, including the effects of system rotation and transpiration on the flow structure. Finally, in Section 6 we shall make our concluding remarks.

2. Dynamical Equations

To date, attention has been largely focused on the incompressible flows governed by the Navier-Stokes equations:

$$\frac{\partial u_i}{\partial t} - \epsilon_{ijk} u_j \omega_k = - \frac{\partial P}{\partial x_i} + \frac{1}{Re} \frac{\partial^2 u_i}{\partial x_j \partial x_j} \tag{1a}$$

$$\frac{\partial u_i}{\partial x_i} = 0 \tag{1b}$$

where Re is the Reynolds number. To satisfy the incompressibility constraint (1b), certain numerical techniques use the Poisson equation for the dynamic pressure:

$$\frac{\partial^2 p}{\partial x_i \partial x_i} = \frac{\partial}{\partial x_i}\left(\epsilon_{ijk} u_j \omega_k\right) \tag{1c}$$

obtained from application of the divergence operator to Eq. (1a).

In the direct simulation (DS) approach, the above equations are solved numerically with appropriate boundary conditions. Aside from errors due to numerical implementation, no further approximations are required. In the large-eddy simulation (LES) technique, the dependent variables are the resolvable portion of the velocity and pressure field. Every flow variable f is decomposed to large-scale and subrid-scale components.

$$f = \bar{f} + f' \tag{2}$$

The large-scale component is defined by

$$\bar{f}(\underline{x}) = \int G(\underline{x},\underline{x}')\, f(\underline{x}')\, d\underline{x}' \tag{3}$$

where G is a filter function with a characteristic length Δ, which is a function of the computational grid resolution. Applying the filtering operation (3) to Eqs. (1a), (1b), or (1c) leads to the exact equations for the large-scale field. The major difference between the filtered and unfiltered equations of the direct simulation is the inclusion of the additional terms associated with the subgrid-scale stresses (SGS) in the governing equations for the large eddies. These terms are modeled to close the system of equations. Different eddy-viscosity models [1, 2, 3] as well as multi-equation models [4] have been successfully used to relate SGS stresses to the resolvable turbulence. These models should display an important feature: as the grid resolution is refined, the characteristic length of the SGS eddies becomes smaller.

In this paper, most of the discussion will be in reference to a Cartesian coordinate system. The x and z (x_1, x_3) axes are parallel to the wall, with x increasing in the mean-flow direction. The y axis is normal to the wall. We shall primarily discuss numerical simulation of flows that are homogeneous or nearly homogeneous in the x and z directions. This is the area where most of the current effort has been concentrated. Some computations of unidirectional flows in cylindrical geometries have been performed [2, 5]. Currently, however, numerical simulation of the turbulent flows in complex geometries involving generalized coordinate systems has not been undertaken. Other notions used in this paper include: δ, the channel

half-width or boundary-layer thickness; U_o, free-stream velocity or centerline velocity in channel; u_τ, shear velocity; U_m, average mean velocity; Re, the Reynolds number based on U_o and δ; Re_τ, the Reynolds number based on u_τ and δ; ν, the kinematic viscosity; y_w, the distance to the wall; and N_i, number of grid points in the x_i-direction.

3. Spatial Resolution Requirements

Generally, numerical simulation of wall-bounded turbulent shear flows requires a large number of grid points in all spatial directions. This requirements is much more stringent than the corresponding one for free-turbulent shear flows (e.g., jets and wakes). The difference stems from physical observations that locally large eddies near the wall are much smaller than those away from the wall. Moreover, in free-turbulent flows, large-scale structures exhibit an appreciable degree of Reynolds number independence, whereas, near the walls, the important large-scale structures decrease in size with increasing Reynolds number.

In the direction normal to the solid boundary, one should and can easily distribute grid points with variable spacings. A sufficient number of grid points should be placed near the wall to resolve the viscous sublayer and the buffer layer. As the Reynolds number increases, more points are required in this region. The grid size can be increased in the regions away from the walls; however, it should be bounded by the Prandtl mixing length ($\sim 0.1\ \delta$).

In the lateral (spanwise) direction, the required number of grid points can be prohibitively large. The difficulty arises due to the fine spacing of the streaky structures [6] in the vicinity of the wall. Kline and his co-workers have shown that streaks play a significant role in the production and dynamics of turbulence in the entire flow field. Therefore, it is important that the numerical simulation of wall-bounded turbulent shear flows resolve these structures or account for their effects. For a limited range of Reynolds numbers, laboratory observations, as well as some quantitative measurements indicate that the mean spacing of the streaks, λ_m, is about 100 wall units, i.e., $\lambda_m^+ = \lambda_m u_\tau/\nu \simeq 100$, and their most probable spacing is about 80 wall units. The mean width of the smaller of the high- and low-speed streaks can be at most $50\ \nu/u_\tau$. In fact, from the measurements of Blackwelder and Kaplan [7], one can deduce that the mean width of the high-speed wall-layer structures is about 20-40 wall units. These values are based on an ensemble of measurements, and, at a given instant, structures with smaller (as well as larger) widths are formed. Therefore, in order to capture the wall structures at their proper scale, it is not unreasonable [8] to require that the computational grid resolution in the spanwise direction be fine enough to resolve eddies with a spanwise extent of 20 wall units. In the numerical integration of the governing nonlinear equations, if we assume that at least four grid points are required to represent an eddy and its

evolution for a short period of time, the computational grid size in the z-direction should be about 5 wall units, i.e., $h_3^+ \simeq 5$. It should be pointed out that this estimate is based on experimental data for moderately low Reynolds number turbulent flows and may not apply at very high Reynolds numbers.

In the absence of physical boundaries in the spanwise direction, the extent of the computational domain in this direction, L_z, should be large enough that artificialities introduced by the use of periodic boundary conditions do not seriously affect the statistics of the flow. Based on two-point correlation measurements [9], L_z should be at least three times the boundary-layer thickness [3]. With these two estimates, the required number of grid points in the z-direction, N_z, is

$$N_z \simeq \frac{3}{5/Re_\tau} = 0.6\ Re_\tau$$

Using the universal velocity-distribution law [10] , we may relate Re to Re_τ:

$$Re = Re_\tau \left(\frac{1}{\kappa} \ell n\ Re_\tau + 5.0 + E \right)$$

where $\kappa \simeq 0.4$, $E \simeq 0$ for channel and pipe flows, and $E \simeq 2.8$ for the boundary layer. Figure 1 shows the required number of grid points in the spanwise direction vs. the Reynolds number for channel flows.

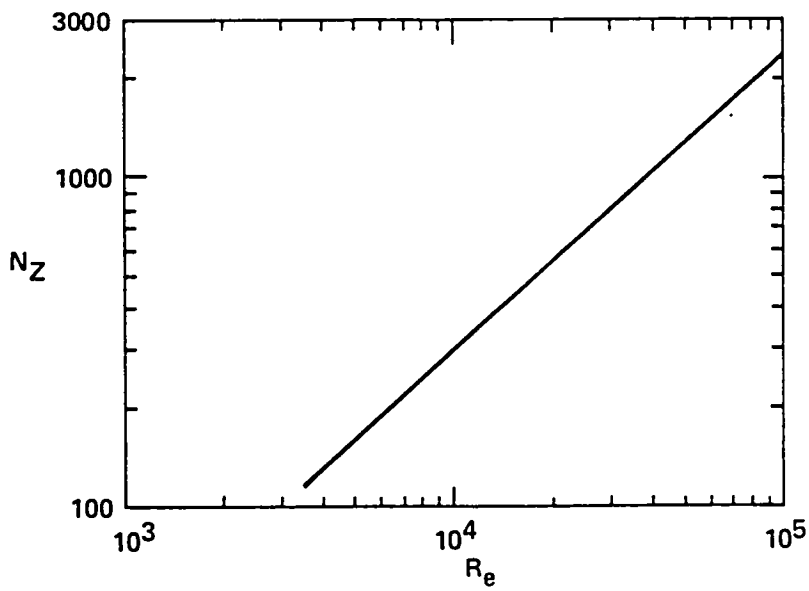

Figure 1. Grid-point requirements in the spanwise direction.

The computational grid requirement is not as stringent in the streamwise direction as in the spanwise direction. Similar considerations of the physics of turbulent boundary layers tend to indicate [3] that, in the streamwise direction, the required number of grid points is about half that for the spanwise direction.*

As an example, for the moderate Reynolds number $Re = 10^4$, 64 nonuniformly spaced grid points appear to be sufficient in the direction normal to the wall(s). For this case, therefore, about 4×10^6 mesh points are necessary to resolve the energetic turbulent structures. The computational effort required for this calculation overly taxes the capabilities of the presently available supercomputers. On the other hand, low Reynolds number flows, such as the channel flow experiment of Eckelmann [11] with $Re = 2800$, is definitely within reach of such computers. For this flow, less than half a million grid points are required.

It is emphasized that the spatial resolution requirements just given are based on the experimentally determined "large" eddy sizes. In the above calculations, one must use subgrid scale (SGS) models to represent the small dissipative eddies. It is difficult to characterize the size of these very small eddies. As a reference, however, we may consider the Kolmogoroff length scale $\eta = (\nu^3/\varepsilon)^{1/4}$ as their typical length scale. For channel flows based on the mean dissipation rate per unit mass for the entire flow field, η can be expressed in the wall units as $\eta^+ = \left[Re_\tau (u_\tau/U_m)\right]^{1/4}$. For the low Reynolds number, $Re = 2800$, that was just considered, η^+ is approximately 2 wall units. Based on the wall value of ε, the limiting value of η^+ is slightly less than 1 (η^+ is exactly equal to 1, if only the dissipation due to mean motion is considered). Clearly, if eddies whose extent is about η^+ in <u>all</u> the spatial directions are to be resolved, the required number of grid points is prohibitively large. Thus, it appears that, with the present computers, <u>direct</u> numerical simulation of wall-bounded turbulent shear flows is not feasible, and calculations should incorporate subgrid scale models to represent the dissipative eddies. However, this conclusion has been based on using η^+ as the characteristic size of the dissipative eddies that must be resolved. The question arises as to whether eddies of this size make significant contributions to the local dissipation rate in turbulent boundary layers. With the available experimental data, it is difficult to answer this question conclusively. A rough estimate of the dissipation spectra obtained from the one-dimensional energy spectra measurements of Bakewell and Lumley [13] seems to indicate that these eddies do make appreciable contributions to the local dissipation rate. Perhaps, the easiest way to answer this question is to attempt a direct simulation of a very low Reynolds number

*This estimate is based on the typical streamwise extent of the wall-layer structures [12]. In visual studies [6], the "lifted" sublayer streaks were observed to oscillate. Depending on the wavelength of these oscillations, more points in the streamwise direction may be necessary.

turbulent channel flow and validate it by detail structural and statistical comparison with the available experimental data.

The demand for a large number of grid points for resolving the wall-layer structures can be significantly reduced by the grid-imbedding technique [14]. One can place a large number of grid points in the x and z directions only in the vicinity of the walls. Since implicit time advancing will generally be used in conjunction with derivatives in the normal direction, this approach is not as convenient to implement as one where the same number of grid points in the x and z directions are used at all the y-locations. However, careful grid imbedding can lead to enormous savings on computer time and storage. If at moderate Reynolds numbers the wall-layer structures are to be resolved at their proper scale, grid imbedding appears to be the only course of action at present.

Another method for alleviating the need for a large number of grid points in the simulation of wall-bounded shear flows is that of Deardorff [1] and Schumann [2]. In this method the flow in the vicinity of the walls is ignored. The calculations are carried out to a point in the logarithmic layer where boundary conditions consistent with the logarithmic velocity distributions are applied. For high Reynolds number flows and certain practical problems, this approach is very promising. With considerably less effort than is required to extend the calculations to the wall, successful comparison of the mean velocity and turbulent stresses with experimental data has been obtained. However, the applicability of these empirical boundary conditions to other flow situations has not been established. Moreover, the effect of perturbations to these boundary conditions on the computed flow field is not yet known. If a two-dimensional, time-dependent "wall function" can indeed be constructed with a sufficient degree of generality, then this type of calculation can be of considerable practical value for the numerical simulation of high Reynolds number, wall-bounded turbulent flows. The calculations that do extend to the wall can serve as a viable testing ground to validate the proposed wall conditions. A novel and inexpensive method for evaluating these conditions is described by Chapman and Kuhn [15]. They calculated the inner region of a turbulent boundary layer by specifying space- and time-dependent boundary conditions at the outer edge of the viscous sublayer. Considerable care was exercised in assuring that these conditions were consistent with the known dynamics of the near-wall turbulence. The appropriate "outer" boundary conditions used in this work can be used as wall conditions in the large-eddy simulation of the outer region of turbulent boundary layers.

4. Numerical Methods

In this section we shall discuss the numerical methods used to solve the three-dimensional, time-dependent, Navier-Stokes equations for wall-bounded turbulent flows. As a result of modeling the subgrid scale stresses, the dynamical equations

in the large-eddy simulation approach are somewhat more complicated than Eqs. (1). However, when eddy-viscosity models are used, these equations can be recast into a form for which virtually identical numerical methods can be used. Equation (1a) can be written as:

$$\frac{\partial u_i}{\partial t} = H_i - \frac{\partial P}{\partial x_i} + \frac{1}{R}\frac{\partial^2 u_i}{\partial x_j \partial x_j} \tag{4}$$

where H_i represents the nonlinear terms (including the subgrid scale terms) and the dependent variables (u_i,P) are to be interpreted either as the full velocity and pressure field in DS, or their resolvable portions in LES.

4.1 Spatial Derivatives

Finite-difference and spectral (pseudospectral) methods have been used to approximate the partial derivatives $\partial/\partial x_i$. Deardorff [1] and Schumann [2] used second-order finite differences in conjunction with staggered grids [16] in all spatial directions. Moin and Kim [3] evaluated partial derivatives in two of the spatial directions (x_1, x_3) pseudospectrally, whereas, derivatives in the direction normal to the walls were evaluated by second-order central-difference formulae. Orszag and co-workers [17, 18], Moin and Kim [19], Kleiser [20] and Taylor and Murdock [21] computed all the spatial derivatives by pseudospectral methods. When using pseudospectral methods, the dependent variables are expressed as a linear combination of a set of orthogonal functions. Fourier series is the appropriate representation of the flow field in the directions for which periodic boundary conditions are used. In other dierctions, orthogonal polynomial decompositions generally lead to a high convergence rate, irrespective of the nature of boundary conditions [22]. For smooth functions, pseudospectral methods are much more accurate numerical differentiators than the conventional second- and fourth-order finite-difference approximations. However, this superiority of the spectral methods may not be very pronounced when turbulent flows which often involve small-scale fluctuations are calculated. In numerical simulation of two-dimensional, Navier-Stokes equations in a periodic box, Herring et al. [23] have systematically compared their results obtained with second-order finite-difference and spectral methods. They showed that spectral calculations are approximately equivalent in accuracy to finite-difference calculations with only twice the resolution in each space dimension. It is quite likely that a more favorable comparison can be obtained if fourth-order finite-difference methods are used. Another important conclusion from their study was that the accuracy or inaccuracy of spectral methods can be deduced from the computed energy spectra, whereas, the spectra obtained from the corresponding finite-difference calculations tend to hide their inaccuracy. To illustrate this property of spectral

methods, we shall consider two numerical simulations of turbulent channel flow, one inadequately resolved and the other with sufficient grid resolution.

Figure 2a shows the one-dimensional lateral energy spectra in the vicinity of the wall ($y_w/\delta = 0.025$) from a turbulent channel-flow simulation at $Re = 13800$, Ref. [3]. In this calculation, the pseudospectral method with 128 grid points was used in the lateral direction. However, for this Reynolds number the resulting computational resolution was not adequate to resolve the wall-layer streaks at their proper scale. The energy accumulation at the high wave-number portions of $E_i(k_3, y_w/\delta = 0.025)$ signals this inadequacy. Note that the longitudinal spectra obtained at the same vertical location (Fig. 2b) do not have energy buildup at high wave numbers. In this calculation, 64 grid points were used in the longitudinal direction. These appear to be sufficient to resolve the streamwise variation of turbulent structures (which, incidentally, suggests that the streamwise grid resolution estimate given in section 3 may be too stringent (see below)). Figure 2c shows the one-dimensional, lateral energy spectra $E_i(k_3, y_w/\delta = 0.389)$ at a distance away from the wall. In this region, the finely spaced near-wall structures are absent, and no resolution problems are expected. This is reflected in the behavior of E_i and the absence of excessive energy buildup at high values of k_3. Figure 3 shows the corresponding near-wall ($y_w/\delta = 0.025$) one-dimensional spectra from a channel flow simulation at the relatively low Reynolds number $Re = 3850$. In this calculation, 128 grid points were also used in the spanwise direction and were apparently sufficient to resolve the wall-layer structures. For this case, no excessive energy accumulation is evident at the high-wave-number end of $E_i(k_3, y_w/\delta = 0.025)$. One should be cautious in using energy spectra as the sole indicator of grid resolution adequacy or inadequacy. Insufficient computational resolution may totally suppress certain instability mechanisms and the subsequent formation and growth of the corresponding turbulent structures. This phenomenon may be concealed from energy spectra.

If the spatial grid resolution is sufficient to resolve all the important scales of motion, spectral or pseudospectral methods certainly are the best possible numerical differentiators. However, in some cases the accuracy afforded by spectral methods should be balanced against inherent inefficiencies in the data-management process and difficulties encountered with application of these methods to complex geometries.

4.2 Explicit Time Advancement

The three momentum Eqs. (4) must be integrated in time, subject to the incompressibility constraint. Explicit methods offer the advantages of low cost per step and ease of formulation and computer programming. In calculations where the wall-layer dynamics have been excluded [1, 2], only explicit time advancement has been

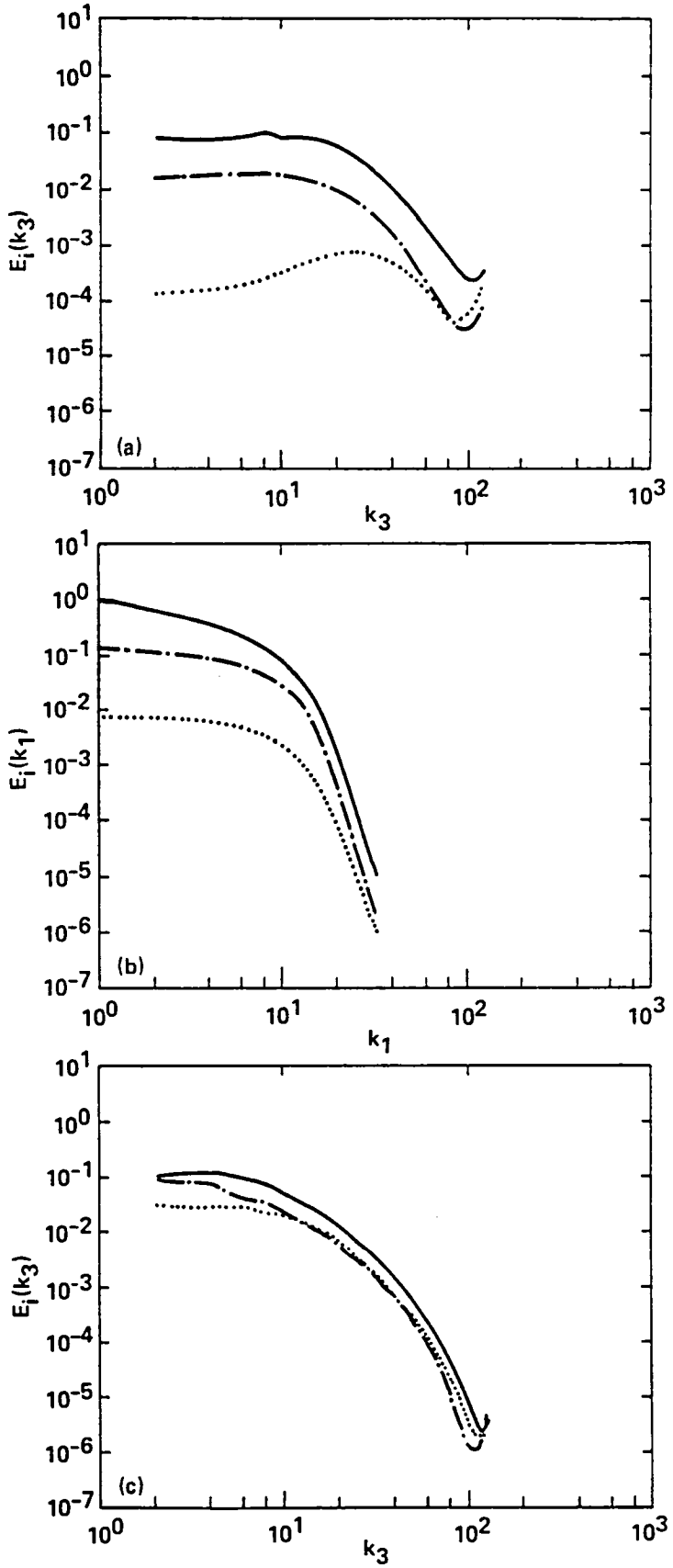

Figure 2. One-dimensional energy spectra at Re 13800. — E_1 spectrum of the streamwise fluctuating velocity; —·—, E_2 spectrum of spanwise fluctuating velocity; ----, E_3 spectrum of normal fluctuating velocity. (a) lateral spectra, $y_w/\delta = 0.025$; (b) longitudinal spectra, $y_w/\delta = 0.025$; (c) lateral spectra, $y_w/\delta = 0.389$. Note that in (a) the ratio of the peak value of E_2 to its value at the highest resolved wave number is only 4.2.

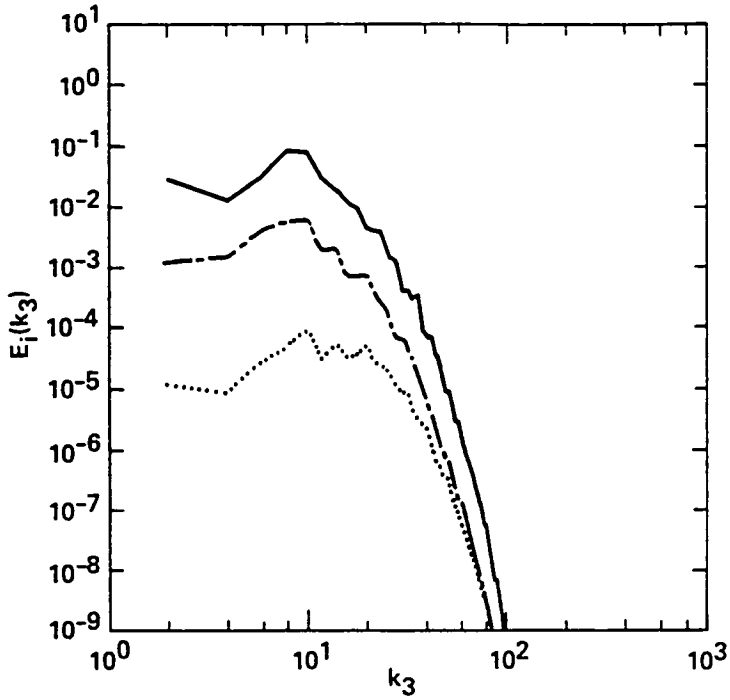

Figure 3. One-dimensional lateral energy spectra at Re = 3850. $y_w/\delta = 0.025$ (see caption of Fig. 2).

used. In these simulations, due to the use of relatively few uniformly or nearly uniformly spaced grid points, the stability restriction (especially those of the diffusion type) on time step is not severe. Both leapfrog and second-order Adams-Bashforth methods have been employed. The latter method has better overall accuracy and stability properties and is more popular now.

To enforce the incompressibility condition at the next time step, usually, the Poisson equation (1c) for pressure is used rather than the continuity equation. For several flow geometries of interest, noniterative, elliptic solvers are available [24] for exact solution (to within round-off errors) of the discretized Poisson equation. It is important, however, to note that the finite-differenced ∇^2 operator for the Poisson equation cannot be chosen arbitrarily [25]. In order to ensure compliance with the incompressibility condition, the numerical gradient operator used to approximate $\partial P/\partial x_i$ in Eq. (4) and the divergence operator must be the same. (When a staggered grid is used, a combination of forward and backward difference schemes for the divergence and the gradient operators also leads to the incompressibility condition.). Except when second-order finite-difference methods on a staggered grid are used, there is some ambiguity with the choice of boundary condition for the Poisson equation (Ref. [19]). Usually, one uses the Neumann boundary condition for pressure (which is obtained from the normal momentum equation). It is also possible to obtain a Dirichlet condition from the boundary evaluation of the tangential momentum equations. In general, the Neumann and Dirichlet problems for pressure

may not have the same solution. It can be shown [19] that, when pseudospectral methods are used in the direction normal to the boundary, in order to satisfy the boundary conditions and the equation of continuity at the wall, it is imperative that both Neumann and Dirichlet conditions for pressure be satisfied. However, only one of them can be used to solve the Poisson equation. This inconsistency leads to serious numerical difficulties if pseudospectral methods are used. With standard finite-difference techniques, although the above ambiguity is still present, the corresponding numerical difficulties can be avoided [26, 27]. If second-order finite-difference methods are used in conjunction with staggered grids, the incompressibility condition at the interior cell adjacent to the boundary provides the additional boundary relation needed to solve the system of algebraic equations for pressure. In this case it is not necessary to extract pressure boundary conditions from the momentum equations.

4.3 Partially Implicit Time Advancement

The calculations that have extended to the wall and applied the no-slip boundary conditions have used semi-implicit numerical methods. These numerical schemes circumvent the prohibitive time-step restrictions arising from the viscous term and the necessity of using very fine mesh spacing in the vicinity of the wall. Moreover, when spectral methods are used to approximate the derivatives in the direction normal to the boundaries, implicit methods provide the means for convenient imposition of boundary conditions. This is because, in contrast to the fully explicit methods, at each time step the problem is treated as a boundary value rather than an initial value problem.

The flows considered to date have been restricted to those that are homogeneous in two space dimensions. The direction of inhomogeneity is normal to the wall(s). Specifically, plane channel flow, pipe flow, axial flow between two concentric cylinders, plane and circular Couette flows have been simulated numerically. For these cases, the use of periodic boundary conditions in the homogeneous directions allows the application of Fourier transforms, which alleviate the need for split or factored-type algorithms. Perhaps, the most direct approach for the solution of Eq. (4) and the continuity equation is to solve them simultaneously. For simulation of turbulent channel flow, Moin and Kim [3, 19] used the second-order Adams-Bashforth method for H_i and the Crank-Nicolson method for $\partial P/\partial x_i$ and $\partial^2 u_i/\partial x_j \partial x_j$ in Eq. (4). This, together with the continuity equation at the new time step, $n + 1$, led to a system of four coupled, linear, partial-differential equations for u_i and P of the form

$$L(u_i^{n+1}, P^{n+1}) = F(u_i^n, u_i^{n-1}, P^n) \tag{5}$$

where the superscripts denote the time step. Fourier transforming Eq. (5) in the x_1 and x_3 directions produces linear, ordinary differential equations of the form

$$\mathscr{L}(\hat{u}_i^{n+1}, \hat{p}^{n+1}) = \hat{F}$$

where $\mathscr{L}$ denotes Fourier transform. To solve these ordinary differential equations, both finite-difference operators on a modified staggered grid [3] and Chebyshev polynomial expansions [19] were used to approximate $\partial/\partial x_2$ and $\partial^2/\partial x_2^2$. The result is a system of algebraic equations for the Fourier transform of the dependent variables at the new time step. For the case where finite-difference operators were used, this system is of block-tridiagonal form; and for the case where Chebyshev polynomials were used, it is nearly block-tridiagonal. Both systems can be solved with $0(N_2)$ operations, where N_2 is the number of mesh points in the x_2-direction.

For their study of transition to turbulence in plane channels and Couette flows, Orszag and Kells [17] used a three-step fractional step method. Chebyshev polynomials and Fourier decomposition were used to represent the dependent variables spatially. In the first step, the Adams-Bashforth method is used for the nonlinear terms, H_i. The result is a set of intermediate velocity field, $\tilde{u}_i^{n+1}$. Next, the pressure correction (incompressibility condition) is applied, leading to another set of intermediate velocity field $\tilde{\tilde{u}}_i^{n+1}$ that satisfies the continuity equation $\partial\tilde{\tilde{u}}_i^{n+1}/\partial x_i = 0$. This step involves solving a Poisson equation for $\tilde{\tilde{u}}_2^{n+1}$ with the boundary conditions $\tilde{\tilde{u}}_2^{n+1} = 0$ at the walls. The velocity field at the new time step is obtained by applying the viscous correction which involves the solution of three Helmholtz equations for the velocity field. The velocity boundary conditions are applied at this stage. This method has a global error of order $0[\Delta t^2 + (1/Re)\,\Delta t]$. Thus, strictly speaking, it is a first-order method. In addition, the velocity field at the new time step does not satisfy the continuity equation. Only the intermediate velocity field, $\tilde{u}_i$, is solenoidal. If the last two steps were interchanged, the velocity field would be divergence-free, but the boundary conditions could not be enforced. Apparently, having the exact boundary conditions was preferred over the continuity equation. Another characteristics of note is that, to solve the Helmholtz equations in the final step using Chebyshev-Fourier expansions, one must transfer the forcing terms in these equations to the wave (Chebyshev-Fourier) space. These terms include $\tilde{\tilde{u}}_i^{n+1}$. Thus, to carry out the transformation, $\tilde{\tilde{u}}_i^{n+1}$ must be defined at the boundaries as well as in the interior of domain. It is necessary, therefore, to concoct boundary conditions for the intermediate velocities, $\tilde{\tilde{u}}_i^{n+1}$.

Recently, Leonard [5] developed a partially implicit method based on a special vector-function decomposition. An important feature of these vector functions is that each vector is solenoidal and satisfies the boundary conditions. When this series expansion for the velocity vector is used in Eq. (4) and the inner product of

the result with a set of adjoint vectors is formed, the pressure terms are eliminated. In fact, since the velocity bases functions satisfy the continuity equation, only two dependent variables per mesh point remain. This leads to considerable savings in computer-memory requirements. Like the previous methods, the nonlinear terms are treated by an explicit method, whereas, the Crank-Nicolson scheme is used for the viscous terms. Leonard and Wray [28] have applied this method to the pipe-flow problem. They rigorously treat the behavior of the flow variables near the computational singularity at the pipe centerline which leads to the use of the Jacobi polynomial expansions in the radial direction. Moser et al. [27] applied this method to plane and curved channel flow problems. In the direction normal to the walls, a particular combination of Chebyshev polynomials was used as bases functions. With this choice, for each Fourier mode, the resulting system of algebraic equations was solved with $O(N_2)$ operations.

4.4 Data Management

Limitations of the high-speed central memory of presently available computers and the large number of grid points required for numerical simulation of turbulent flows necessitate the use of secondary memory. Generally, the entire data base must reside on secondary memory (SM) and only portions of it are successively transferred to the core memory (CM) for processing. In order to minimize the data transfer (I/O) time, an efficient data-management algorithm should be an essential part of each computer program.

The particular choice of data-management technique depends on the numerical method and the computer used for the calculations. However, all the algorithms have the objective of overlapping the data transfer from SM to CM with arithmetic operations. It is also important to minimize the number of passes over the data base. In general, one or two passes are required at each time step.

As an example of a data-management algorithm, we consider the scheme employed in Ref. [3]. In order to solve Eq. (6), a two-pass, double-buffer, data-management algorithm was used. In the first pass over the data base, the required pressure-velocity data from previous time steps are transferred to CM, and $\hat{F}$ (Eq. (6)) is computed and transferred to SM. Since second-order finite-difference formulas were used to approximate the derivatives in the x_2-direction, each time only three $(x_1 - x_3)$ planes of data are required to compute $\hat{F}$ in one plane. In the second pass, $(x_2 - x_3)$ planes of $\hat{F}$ were transferred to CM, and the block-tridiagonal system was solved. Note that, with this algorithm, the data were accessed in two different ways — first in the $x_1 - x_3$ planes and then in the $x_2 - x_3$ planes. Since the data are stored sequentially in, say, the $x_1 - x_3$ planes, the second access ($x_2 - x_3$ planes) is nonsequential; therefore, it is not as efficient. Alternatively, another data-management scheme can be used for solving the same set

of equations. With this algorithm, in the first pass, in addition to computing $\hat{F}$, the forward sweep portion of the Gauss-elimination process can also be performed. In the second pass, the backward sweep portion is performed again, using $x_1 - x_3$ planes. Thus, the data base is accessed sequentially. In fact, the entire process can usually be accomplished with only one pass through the data base per time step [30]. It should be pointed out that, if pseudospectral rather than finite-difference methods are used in the x_2-direction, two passes through the data base (one of them nonsequential) are required.

We emphasize that the numerical methods discussed here have been largely designed for and applied to the simplest wall-bounded, turbulent shear flows, namely, those that are homogeneous in two spatial directions. The flow homogeneity has led to the use of periodic boundary conditions as a reasonable approximation to the unknown flow conditions at the "open" boundaries. The use of Fourier transforms converts the task of solving a partial differential equation to that of solving a set of uncoupled ordinary differential equations. This is a very significant fringe benefit associated with periodic boundary conditions. In order to calculate flows with two or more directions of inhomogeneity, in addition to having to specify the unknown (turbulent) inflow and outflow conditions, one should use split- or factored-type algorithms. An adaptation of the fractional step method appears to be an attractive candidate for this purpose.

5. Results

To illustrate the versatility and usefulness of the aforementioned calculations, we briefly present here a selection of recent results from the large-eddy simulation of wall-bounded turbulent flows. The main calculations were performed on the ILLIAC IV computer with $64\times63\times128$ grid points in the x, y, and z directions, respectively. The total computational time ranged from 20 hours to 92 hours.

Figure 4 shows the mean velocity profile, $\langle\bar{u}\rangle$, from numerical simulation of turbulent channel flow at $Re = 13800$, Ref. 3. Different symbols represent calculations with different grid resolutions and different sizes of the computational box in the x- and z-directions, where periodic boundary conditions are used. The calculations have predicted the logarithmic region with the proper slope. The agreement with the experimental data [31] is good. The distributions of the Reynolds stresses (Fig. 5) and higher-order statistics are also in good agreement with measurements. The contribution of subgrid scale turbulence to second- and higher-order statistical correlations is appreciable only in the vicinity of the walls. This is a consequence of the grid-resolution inadequacy in this region to represent the wall-layer turbulence structures at their proper scale. Figure 6 shows a contour plot of the instantaneous normal component of vorticity fluctuations, $\omega_2 = (\partial w/\partial x - \partial u/\partial z)$ in an $x - z$ plane close to the wall ($y^+ \simeq 6$). It is clear that, in accordance

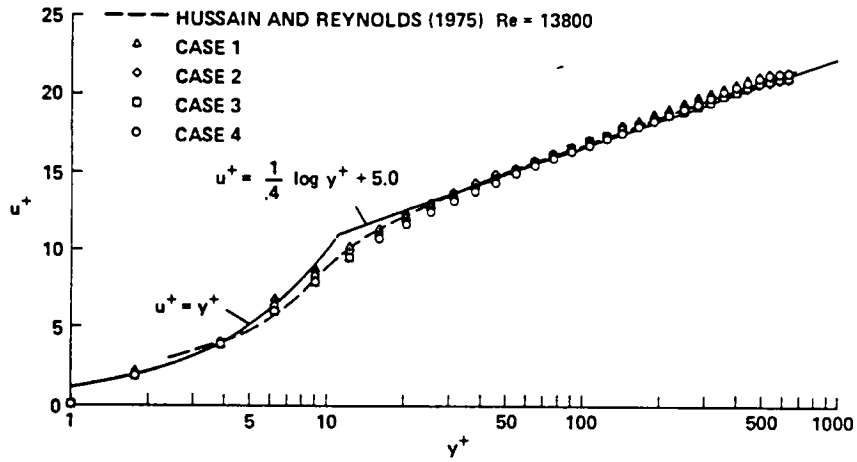

Figure 4. Mean velocity profile from four computed cases and comparison with experimental data. Four results are obtained from using different computational grids.

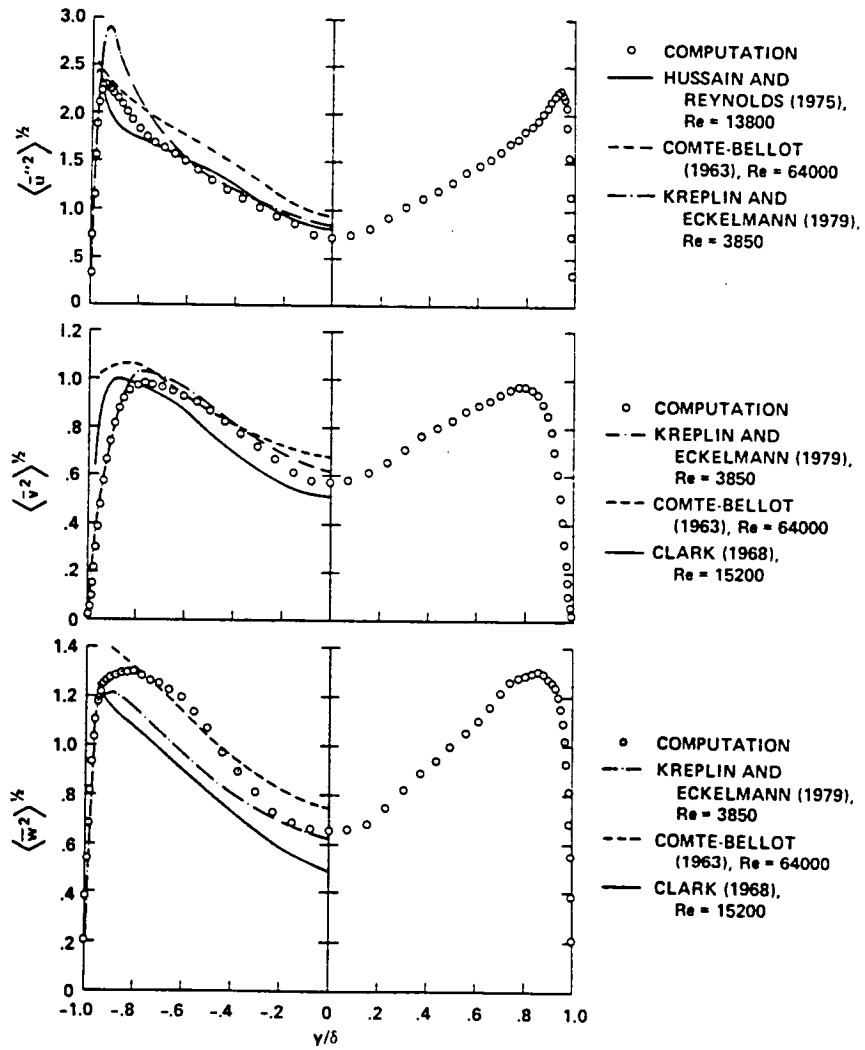

Fig. 5 Resolvable turbulence intensities and comparison with experimental data. The intensities are non-dimensionalized with the shear velocity, u_τ.

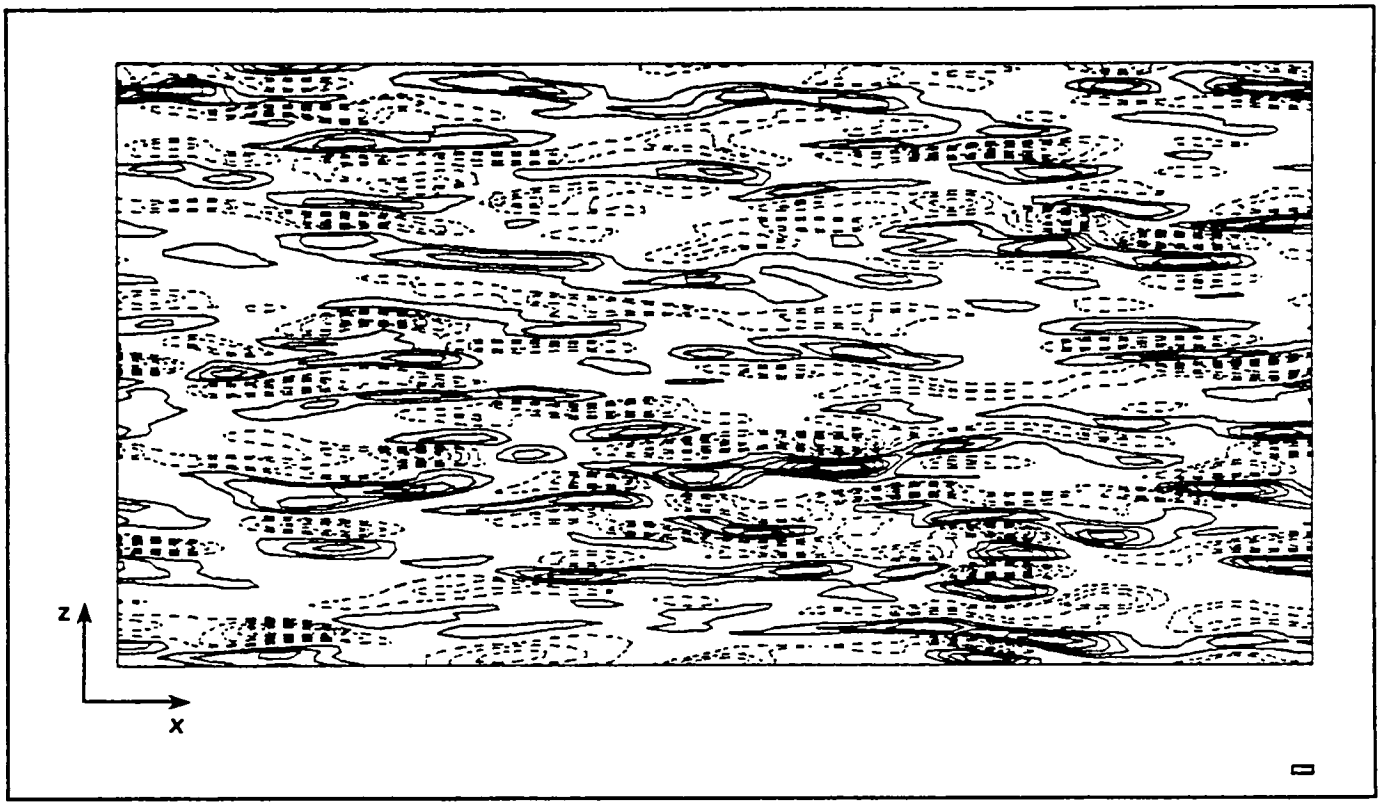

Figure 6. Contours of ω_2 in the (x, z)-plane at $y^+ = 6.26$. The rectangle on the lower right-hand corner of the figure represents the computational grid cell in the (x, z) planes. The streamwise extent of the figure is $2\pi\delta$ and its spanwise extent is $\pi\delta$.

with experimental measurements [6], this region is composed of flow structures which are long in the flow direction and narrow in the spanwise direction. The rapid spanwise variation of ω_2 is due to the existence of elongated regions of high-speed fluid ($(\bar{u} - \langle\bar{u}\rangle) > 0$) located adjacent to the low-speed regions [6, 3]. This figure is a vivid display of that particular characteristic of wall-bounded turbulent shear flows which requires a large number of grid points in the lateral direction. As was pointed out in section 3, in this calculation, the spanwise grid resolution was not adequate to resolve the wall-layer streaks at their proper scale. However, it is quite significant that, in spite of this, the computed flow field did display the streaky structures but at a larger scale.

The data generated from these calculations are currently being used to study the physical structure and dynamics of turbulent channel flow. In one study, for example, our aim is to identify large-scale, energetic structures in the flow field. In particular, we wanted to investigate the frequency and dominance of horseshoe or hairpin vortices that have been observed to originate at the wall and extend to outer regions with the characteristic inclination angle 40° - 50° (see, e.g., Ref. [32].) The vorticity field at several points in time was computed. At each grid point in various $x - z$ planes, the angle $\theta = \tan^{-1}(\omega_2/\omega_1)$, and

$|\omega_{12}| = (\omega_1^2 + \omega_2^2)^{1/2}$ was calculated. Figure 7 shows the resultant distribution at $y_w/\delta = 0.2$. The contribution from each grid point was weighted by $|\omega_{12}|$. Indeed, the distribution attains its maximum at $\theta = 45°$. However, the probability of finding vorticity vectors with inclination angle in the range $0 \leqslant \theta \leqslant 90°$ is also appreciable. A detailed description of the results of this study will be presented elsewhere. In another investigation, Kim [33] has used the computed velocity-pressure field to examine the structure of the flow by conditional sampling techniques. Figure 8 shows the conditionally averaged, streamwise velocity obtained by using the VITA technique [7]. It is remarkably similar to the experimental results of Blackwelder and Kaplan [7]. The figure displays the burst and sweep events and their vertical extent. Kim has extended the experimental findings utilizing conditionally averaged pressure, vorticity, and the spanwise velocity component.

By simple modifications of the channel flow code described above, the effects of transpiration and spanwise rotation on the flow were computed. In the former case, uniform blowing through one wall and uniform suction at the same rate was applied through the other wall. Figure 9 shows that, in agreement with experimental measurements, the calculations predict the wall-shear-stress diminution caused by blowing

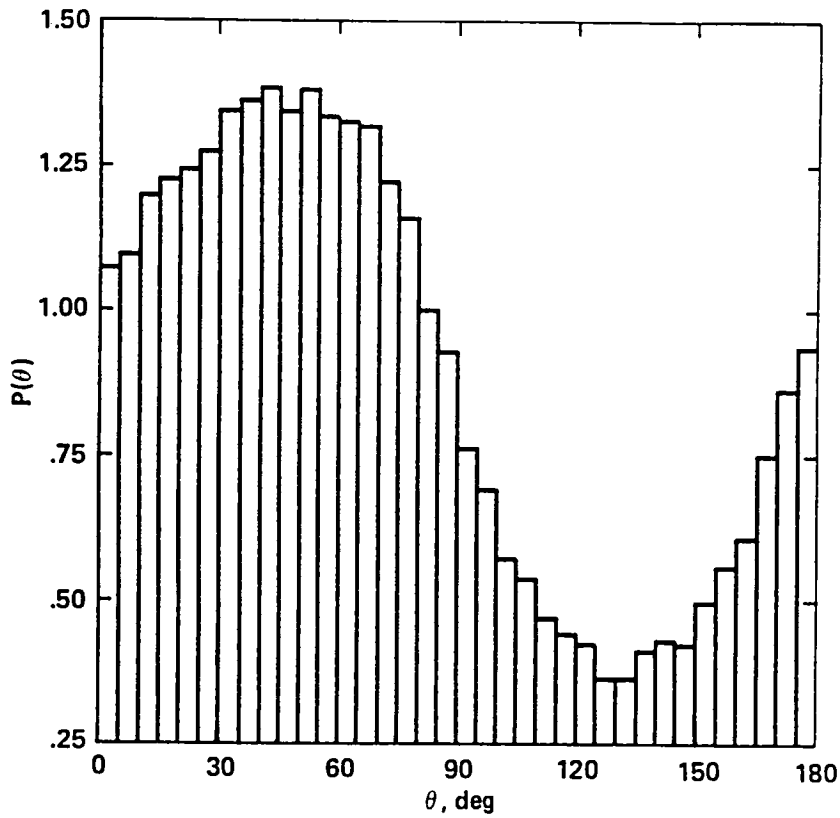

Figure 7. Distribution of the inclination angle of vorticity vectors (weighted by $|\omega_{12}|$) at $y_w/\delta = 0.2$.

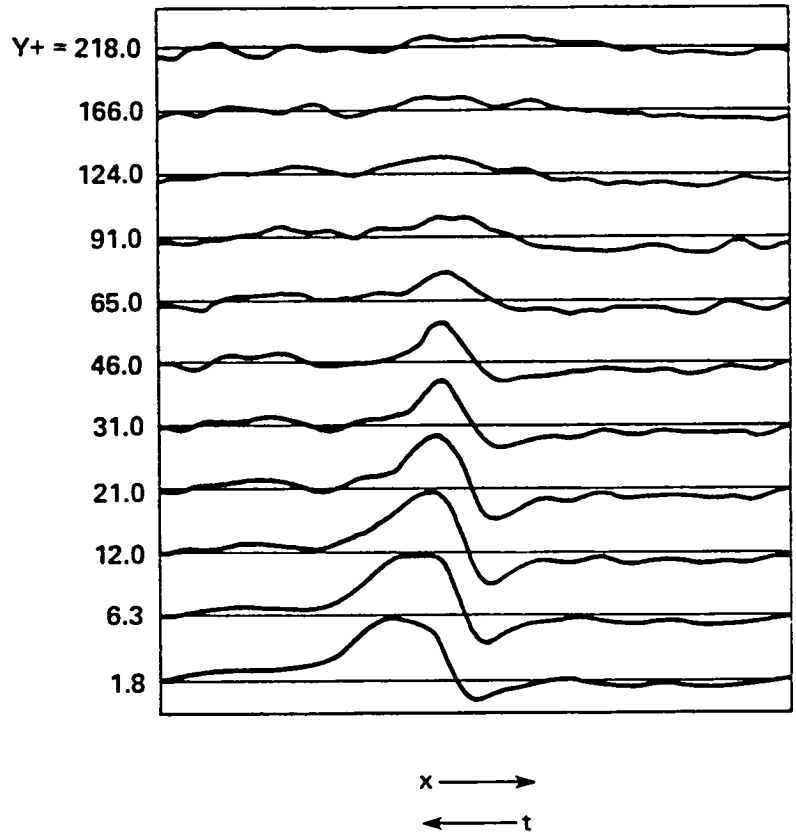

Figure 8. Conditionally averaged streamwise velocity fluctuations at various distances from the wall.

and its augmentation resulting from suction. Other features of the computed flow field, such as the effect of transpiration on the distribution of Reynolds stresses, are also in agreement with measurements. In the case of the rotating channel, the computational results [35] are in good agreement with the experimental data [36] and reproduce the detailed structural features of the flow as observed by flow-visualization techniques. The primary effect of rotation is that the flow is stabilized on one wall and destabilized on the other. The skin friction is reduced on the "stable wall" and is increased on the "unstable wall" (Fig. 10). One of the objectives of these studies was to examine the relationship between the changes in skin friction and flow structure in the vicinity of the wall. In both flows, it has been shown that there is a definite correlation between the characteristic dimensions of the wall-layer streaks and viscous drag.

6. Concluding Remarks

The results of the numerical simulation of wall-bounded turbulent shear flows have been most encouraging. For geometrically simple cases, it has been possible to predict many of the statistical and time-dependent features of the flows considered. The potential of these calculations for increasing our understanding of the physics of turbulent boundary layers is just beginning to be tapped.

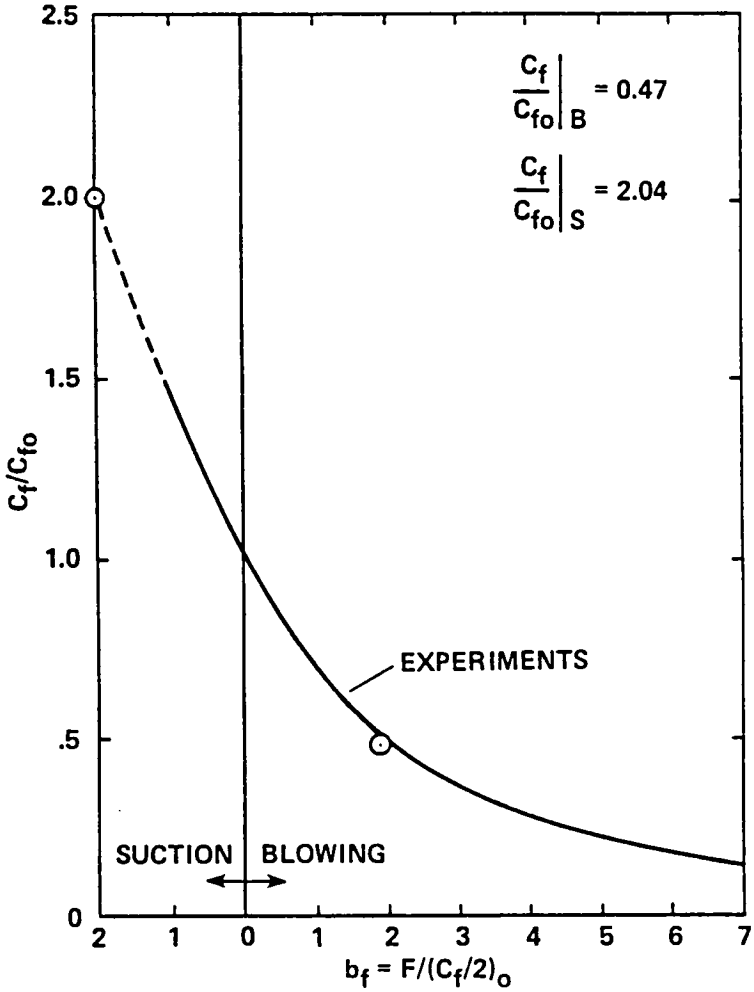

Figure 9. Ratio of friction coefficient to friction coefficient without transpiration, plotted as a function of a modified blowing parameter b_f [34]. ⊙, computation; —— correlation curve of the experimental data; ----, linear extrapolation of the experimental correlation curve.

The large number of grid points required to resolve the wall-layer structures is a formidable hindrance to numerical simulation of high Reynolds number flows. The grid-imbedding technique can significantly ease this burden. Consideration of the bursting frequency and the frequency spectra of streamwise velocity fluctuations [37, 13] indicates that, for moderate Reynolds numbers, it may be possible to perform accurate LES calculations with larger time steps than is currently permitted by numerical stability restrictions. Thus, further improvements in numerical methods are likely to yield high dividends.

Extension to more complex geometries requires progress in our ability to prescribe turbulent inflow and outflow boundary conditions. Another practical difficulty in calculating these inhomogeneous flows is acquiring adequate ensemble averages. In contrast to homogeneous flows, one cannot integrate turbulence quantities over spatial grid points to secure a better statistical sample. To obtain adequate statistics, the only resort is time-averaging or, in the case of

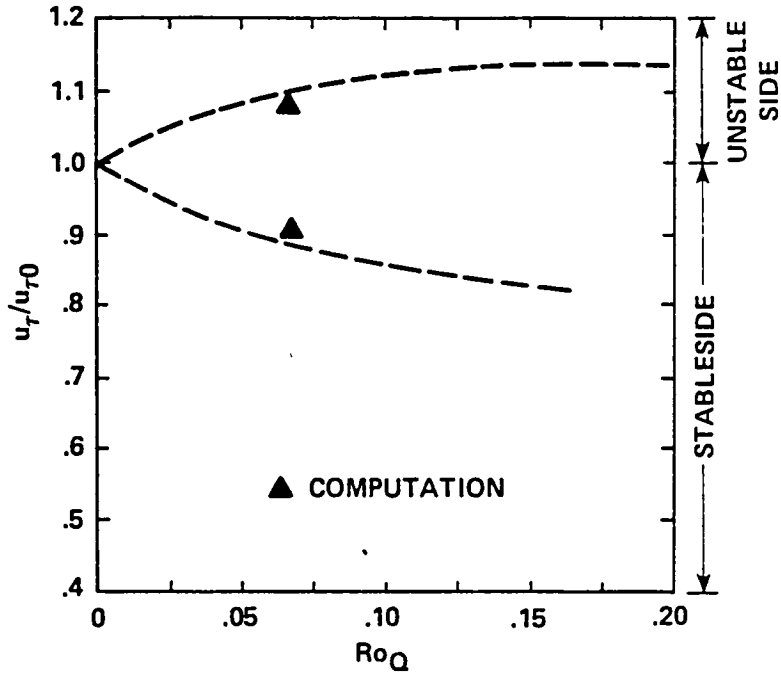

Figure 10. Ratio of the shear velocity to the shear velocity without rotation, plotted as a function of the rotation number. ▲, computation [35]; ----, curve fit to the experimental data [36].

nonstationary flows, averaging over several independent calculations. In both cases, the computational cost is significantly higher than for flows with one or two directions of homogeneity.

Acknowledgments

I am grateful to J. Kim for helpful discussions and for generously providing me with some results of his unpublished work. Useful discussions with A. Leonard are also appreciated.

References

1. Deardorff, J. W., 1970. A Numerical Study of Three-Dimensional Turbulent Channel Flow at Large Reynolds Numbers. J. Fluid Mech., 41, 453-480.

2. Schumann, U., 1975. Subgrid Scale Model for Finite Difference Simulations of Turbulent Flows in Plane Channels and Annuli. J. Comp. Phys., 18, 376-404.

3. Moin, P., and J. Kim, 1982. Numerical Investigation of Turbulent Channel Flow. J. Fluid Mech., 118.

4. Deardorff, J. W., 1973. The Use of Subgrid Transport Equations in a Three-Dimensional Model of Atmospheric Turbulence. J. Fluids Engr., 95, 429.

5. Leonard, A., 1981. Divergence-Free Vector Expansions for 3D Flow Simulations. Bull. of Amer. Phys. Soc., 26, 9, 1247.

6. Kline, S. J., W. C. Reynolds, F. A. Schraub, and P. W. Rundstadler, 1967. The Structure of Turbulent Boundary Layers. J. Fluid Mech., 30, 741-773.

7. Blackwelder, R. F., and R. E. Kaplan, 1976. On the Wall Structure of Turbulent Boundary Layer. J. Fluid Mech., 76, 89.

8. Gupta, A. K., J. Laufer, and R. E. Kaplan, 1971. Spatial Structure in the Viscous Sublayer. J. Fluid Mech., 50, 493.

9. Comte-Bellot, G., 1963. Contribution a l'Etude de la Turbulence de Conduite.

10. Hinze, J. O., 1975. Turbulence, McGraw-Hill, Inc., 2nd ed.

11. Eckelmann, H., 1974. The Structure of Viscous Sublayer and The Adjacent Wall Region in a Turbulent Channel Flow. J. Fluid Mech., 65, 439.

12. Clark, J. A., and E. Markland, 1971. Flow Visualization in Turbulent Boundary-Layers. Proc. ASCE, J. Hydraulics Div., 97, 10, 1653-1664.

13. Bakewell, H. P., and J. L. Lumley, 1967. Viscous Sublayer and Adjacent Wall Region in Turbulent Pipe Flow. Phys. Fluids, 10, 1880.

14. Chapman, D. R., 1979. Computational Aerodynamics Development and Outlook. AIAA J., 17, 1293-1313.

15. Chapman, D. R., and G. D. Kuhn, 1981. Two Component Navier-Stokes Computational Model of Viscous Sublayer Turbulence. AIAA Paper 81-1024, AIAA 5th CFD Conf., Palo Alto, Calif.

16. Harlow, F. H., and J. E. Welch, 1965. Numerical Calculation of Time-Dependent Viscous Incompressible Flow. Phys. Fluids, 8, 2182.

17. Orszag, S. A., and L. C. Kells, 1980. Transition to Turbulence in Plane Poiseulle and Plane Couette Flow. J. Fluid Mech., 96, 159.

18. Patera, A. T., and S. A. Orszag, 1980. Transition and Turbulence in Planar Channel Flows. Lecture Notes in Physics (W. C. Reynolds, and R. W. MacCormac, eds.) 114, 329, Springer-Verlag.

19. Moin, P., and J. Kim, 1980. On the Numerical Solution of Time-Dependent Viscous Incompressible Fluid Flows Involving Solid Boundaries. J. Comp. Physics, 35, 381-392.

20. Kleiser, L., 1979. Solution of Coupled Velocity-Pressure Equations in the Fourier-Chebyshev Spectral Method for Incompressible Flows. Private communication.

21. Taylor, T. D., and J. W. Murdock, 1981. Application of Spectral Methods to the Solution of Navier-Stokes Equations. Comp. and Fluids, 9, 255.

22. Orszag, S. A., 1971. Galerkin Approximations to Flows Within Slabs, Spheres, and Cylinders. Phys. Rev. Lett., 26, 1100.

23. Herring, J. R., S. A. Orszag, R. H. Kraichnan, and D. G. Fox, 1974. Decay of Two-Dimensional Homogeneous Turbulence. J. Fluid Mech., 66, 417.

24. Buzbee, B., G. Goulub, and C. Nielsen, 1970. On the Direct Methods for Solving Poisson's Equation. SIAM J. Numer. Anal., 7, 627.

25. Shaanan, S., J. H. Ferziger, and W. C. Reynolds, 1975. Numerical Simulation of Turbulence in the Presence of Shear. Report No. TF-6, Dept. of Mech., Engrg., Stanford University.

26. Moin, P., W. C. Reynolds, and J. H. Ferziger, 1978. Large Eddy Simulation of Incompressible Turbulent Channel Flow. Report No. TF-12, Dept. of Mech. Engrg., Stanford University.

27. Kim, J., and P. Moin, 1979. Large Eddy Simulation of Turbulent Channel Flow --ILLIAC IV Calculation. In Turbulent Boundary Layers--Experiments, Theory, and Modeling, The Hague, Netherlands. AGARD Conf. Proc. no. 271.

28. Leonard, A., and A. Wray, 1982. Numerical Solution of Three-Dimensional Transitional Flow in a Pipe. Proc. of this conference.

29. Moser, R. D., A. Leonard, and P. Moin, 1982. To be published.

30. Wray, A., and M. Y. Hussaini, 1980. Numerical Experiments in Boundary-Layer Stability. AIAA Paper 80-0275, AIAA 18th Aerospace Science Meeting, Pasadena, Calif.

31. Hussain, A.K.M.F., and W. C. Reynolds, 1975. Measurements in Fully Developed Turbulent Channel Flow. J. Fluids Engrg., 97, 568-578.

32. Head, M. R., and P. Bandyopadhyay, 1981. New Aspects of Turbulent Boundary-Layer Structure. J. Fluid Mech., 107, 297.

33. Kim, J., 1982. Stanford University, to be published.

34. Kays, W. M., 1972. Heat Transfer to the Transpired Turbulent Boundary-Layer. Int. J. Heat and Mass Transfer, 15, 1023.

35. Kim, J., 1982. Stanford University, to be published.

36. Johnston, J. P., R. M. Halleen, and D. K. Lezius, 1971. Effects of Spanwise Rotation on the Structure of Two Dimensional Fully Developed Turbulent Channel Flow. J. Fluid Mech., 56, 533.

37. Rao, K. N., R. Narasimha, and M. A. Badri Narayanan, 1971. The Bursting Phenomenon in a Turbulent Boundary Layer. J. Fluid Mech., 48, 339.

1. Report No. NASA TM- 84259	2. Government Accession No.	3. Recipient's Catalog No.
4. Title and Subtitle NUMERICAL SIMULATION OF WALL-BOUNDED TURBULENT SHEAR FLOWS*		5. Report Date 6. Performing Organization Code
7. Author(s) Parviz Moin		8. Performing Organization Report No. A-8902
9. Performing Organization Name and Address NASA Ames Research Center Moffett Field, California 94035		10. Work Unit No. T-4209 11. Contract or Grant No.
12. Sponsoring Agency Name and Address National Aeronautics and Space Administration, Washington, D.C. 20546		13. Type of Report and Period Covered Technical Memorandum 14. Sponsoring Agency Code

15. Supplementary Notes *Presented by invitation at the 8th International Conference on Numerical Methods in Fluid Dynamics. Aachen, W. Germany, June 28 - July 2, 1982
Point of contact. Parviz Moin, M.S. 202A-1, NASA Ames Research Center, Moffett Field, California 94035 (415) 965-5127, FTS 448-5127.

16. Abstract

This paper reviews some recent developments in three-dimensional, time-dependent numerical simulation of turbulent flows bounded by a wall. Both direct and large-eddy simulation techniques are considered within the same computational framework. The computational spatial-grid requirements as dictated by the known structure of turbulent boundary layers are presented. The numerical methods currently in use are reviewed and some of the features of these algorithms, including spatial differencing and accuracy, time advancement, and data management are discussed. A selection of the results of the recent calculations of turbulent channel flow, including the effects of system rotation and transpiration on the flow are included.

17. Key Words (Suggested by Author(s))	18. Distribution Statement
Fluid mechanics Turbulence Numerical simulation Wall-bounded shear flows	Unlimited Subject category - 34

19. Security Classif. (of this report)	20. Security Classif. (of this page)	21. No. of Pages	22. Price*
Unclassified	Unclassified	23	A02

*For sale by the National Technical Information Service, Springfield, Virginia 22161